

RESERVE THIS SPACE

***In silico* Strategies for Modeling Stereoselective Metabolism of Pyrethroids**

Daniel T. Chang^{1*}, Michael-Rock Goldsmith¹, Rogelio Tornero-Velez¹, Yu-Mei Tan¹, Christopher M. Grulke¹, Elin M. Ulrich¹, Andrew B. Lindstrom¹, Melissa A. Pasquinelli², James R. Rabinowitz³ and Curtis C. Dary⁴

¹National Exposure Research Laboratory, US Environmental Protection Agency, Research Triangle Park, NC 27711, USA

²North Carolina State University, Raleigh, NC 27695, USA

³National Center for Computational Toxicology, US Environmental Protection Agency, Research Triangle Park, NC 27711, USA

⁴National Exposure Research Laboratory, US Environmental Protection Agency, Las Vegas, NV 89119, USA

[*chang.daniel@epa.gov](mailto:chang.daniel@epa.gov)

ABSTRACT

In silico methods are invaluable tools to researchers seeking to understand and predict metabolic processes within PBPK models. Even though these methods have been successfully utilized to predict and quantify metabolic processes, there are many challenges involved. Stereochemical processes are a particular challenge requiring computational methods to elucidate 3D structures and their inherent conformational dependence within a biological context. Methods to estimate stereoselective metabolic hydrolysis in mammals are presented to aid PBPK modelers in determining qualitative as well as quantitative relationships among the chiral pyrethroid pesticides. We illustrate a case example of rat serum carboxylesterase (rsCE)-mediated hydrolysis of 27 pyrethroid stereoisomers elucidated through a proposed three-step *in silico* workflow. The methodology involves (i) a pharmacophore structural qualifier/filter to determine whether or not a particular stereoisomer is indeed a viable substrate, and (ii) a mechanism-specific quantitative structure activity relationship (QSAR) to predict metabolic rate constants. Our strategy extends the utility of pharmacophore filters in the reduction of misclassification of mechanistically competent substrates, while strengthening the utility of QSAR models within PK/PD model development.

INTRODUCTION

Accurate characterization of biochemical processes in pharmacokinetic (PK) modeling is critical for correctly interpreting and predicting health outcomes in risk assessment(1-8). Physiologically-based pharmacokinetic (PBPK) models extend PK modeling techniques to include organ tissue volume, mass, and blood flow(9). As such, PBPK models provide greater correspondence between *in vitro* and *in vivo* derived parameters than single compartment PK models. However, PBPK models are parameter intensive requiring both species and chemical-specific data. The use of *in silico* procedures to predict parameters can

facilitate model development by providing plausible estimates, or priors (Bayesian), amenable to statistical analysis(10-12).

Specific challenges exist in modeling metabolism. Chirality presents one of these challenges. The macromolecular structure and function of DNA and encoded proteins are dependent on chirality of individual subunits and thereby “selective” to specific stereoisomeric configurations of substrates when describing such interactions.(13-15) A recent review(16) has commented on the implication of chiral pesticides in an environmental context. In this chapter, we offer an *in silico* workflow whereby a small *in vitro* dataset can be utilized to develop *a priori* estimates of stereoselective hydrolysis rates based mechanistic understanding of the process for stereoselective metabolism. We show how stereospecific kinetics can be ascertained, and how chemoinformatics and structural bioinformatics can be used to develop meaningful Quantitative Structure-Activity Relationships (QSAR).

Pyrethroids and chirality

Determining the metabolic rates and mechanisms of detoxification of pyrethroids is critical for developing PBPK models to test exposure route scenarios and to account for biomarkers(17-21). In previous work(17), we have explored docking calculations as a viable means of elucidating relative stereoselectivity of carboxyesterases for pyrethroid stereoisomers. Knaak *et al.*(18) have recently reviewed the current state of PK/PD parameters for pyrethroid insecticides as they relate to human risk assessment. Pyrethroids exhibit a variety of chiral centers influencing selective phase I biotransformation (hydrolytic ester cleavage) by serine esterases(22-27). Structurally, up to three chiral centers may be present with a total of up to 8 stereoisomeric configurations referred to as α -R or α -S(22, 28). The target (insect) and non-target (mammalian) toxicity of pyrethroids is dependent on the stereochemistry(29-30). Observations on variation in

potencies (neurotoxic effects of type-I and type-II pyrethroids)(29-30), in stereoselective hydrolysis rates(23-25), and species differences in metabolism(25, 31-33) have been reported. Type I pyrethroids (*i.e.* lacking the α -cyano group in the alcohol moiety) with *1R* configuration or Type II pyrethroids (*i.e.* cyanopyrethroids) with α -*S* configuration possess high insecticidal activity. The presence of the same configuration at the C1 and α -C in general also elicits more potent acute neurotoxicity in mammals, though the configuration at cyclopropane C3 of the non-cyanopyrethroids also strongly influences toxicity. For example, both [*1R, cis*]-permethrin and [*1R, trans*]-permethrin possess similar insecticidal activity, but only [*1R, cis*]-permethrin is toxic to mammals(30). Differentiation between active and inactive insecticidal stereoisomers and their effects on off-target species resides in the elucidation of their stereospecific metabolism as single stereoisomers may be active for the target species while inactive stereoisomer may be toxic in off-target species.

This rationale forms the basis for our interest in studying enantiopure and enantiomerically enriched products of pyrethroids – *i.e.*, a reduction of isomeric “ballast”(34). Since one of the largest confounding variables in the accurate interpretation of pyrethroid pharmacokinetics is chirality, interpreting stereochemistry of pyrethroids in the context of metabolism of a set of pyrethroid stereoisomers and differentiating the effect of a given isochiral configuration on a set of congeneric pyrethroids are two objectives of this study. Upon resolution of this issue, the subsequent elucidation of structure activity relationships between the stereoisomeric series of a chemical and different chemistry with isochiral configurations would enable a rational mechanism to aid in modeling racemic stereoisomeric mixtures.

METHODS

A ligand-based pharmacophore method was employed to explore our limited *in vitro* dataset example. Pharmacophore models have been developed to identify potential ligands for a variety of receptors(35-37). Pharmacophores, as defined by IUPAC, are “an ensemble of steric and electronic features that are necessary to ensure the optimal supramolecular interactions with a specific biological target and to trigger (or block) biological responses(38).” These “features” range from H-bonding and hydrophobic interactions to projected vector interactions such as acceptor/donor/ π -interaction motifs. Multi-feature pharmacophore models can be facilely developed from available 3D molecular structure (*i.e.*, classification of putative substrates vs. non-substrates) and common features within a given set of ligands. Shape information (*i.e.*, van der Waals volume) from ligand conformations can also be incorporated for further selectivity(39). The success of a pharmacophore model is gauged on maximizing true outcomes from a given dataset while minimizing false outcomes. True outcomes (either positive or negative) are defined as “active” or “inactive” molecules in a confusion matrix sense(40). In the case of our dataset, we assume that putative substrates are “actives” with a positive outcome, while putative non-substrates are “inactives” with a negative outcome.

In silico workflow

The ligand-based pharmacophore approach schematically depicted in Figure 1 consists of three sequential steps: i) dataset classification with energy constrained stereoisomeric conformations, ii) a pharmacophore query on flexible alignment of actives to elucidate similar features based on the conformer search, and iii) mechanistic based QSAR model is developed from pharmacophore filtered datasets of active and inactive 2D and/or explicit 3D molecular descriptors. At a minimum, the *in vitro* or *in vivo* data requirement for this process is stereoselective. The span

of specific activities is classified as either “active” or “inactive” for the putative outcome being modeled. Model queries are scored and ranked based on performance (*i.e.*, relative accuracy) correctly identifying actives and inactives within a training set. The pharmacophore features can also be corroborated against any available docking results and/or used in docking studies. Homology modeling can be employed if no known crystallographic structure is available.

In vitro dataset and specific activity/outcome

Our *in silico* work is trained on the dataset from Chen *et al.*(41) containing 27 stereoisomerically differentiated *in vitro* data points. Each stereoisomer was observed to undergo differential hydrolytic cleavage around the ester linkage via rat serum carboxylesterase (rsCE). Both the rate of serum carboxylesterase hydrolysis (k_h) and half-life ($t_{1/2}$) data were experimentally determined for Sprague-Dawley (SD) and Long-Evans (LE) rats. We selected the larger stereochemical dataset for the SD rat. We found negligible differences in the stereoisomeric rsCE metabolism between the two strains (*i.e.*, slightly shorter half-lives observed in the LE dataset vs. the SD dataset). For reference, the log values of the specific metabolic reaction parameters for SD rats (k_h and $t_{1/2}$) are plotted in Figure 2. The indices along the ordinate axis in Figure 2 directly correspond to the stereochemical structures listed.

Computational details

All computations were performed using Molecular Operating Environment software MOE(42). All of the individual stereoisomers listed in Figure 3 were constructed and geometrically optimized within MOE using the MMFFx(43) force-field to an energy gradient of <0.01 (kcal/mol/Å). The compiled structural dataset was subject to a conformational search. Utilizing a low-mode molecular dynamics search algorithm(44-45), a maximum of 500 lowest energy conformations satisfying a strain

energy cutoff (ΔE) of less than 7 kcal/mol were retained for each stereoisomer to be used in subsequent pharmacophore and QSAR model development. Pharmacophore model development was performed within the Pharmacophore Elucidator module of MOE after performing a user-defined classification of the dataset. A genetic algorithm descriptor optimizer (QuaSAR-Evolution) as employed within the AutoQuaSAR scientific vector language (SVL) script module(46) was utilized to develop QSAR models. A standard leave-one-out (LOO) cross validation method was employed to rank the relative performance of the generated QSAR models.

RESULTS AND DISCUSSION

Dataset preparation

A training set of 27 stereoisomerically differentiated pyrethroid structures was constructed (Figure 3). Type II pyrethroids ($n = 22$) are fairly evenly represented by 10 α -*R* and 12 α -*S* configurations. The training set is evenly distributed between 14 and 13 incidences of *cis/trans* configurations (differentiated about the C1-C3 cyclopropane ring bond). Furthermore, four acid and three alcohol moieties are characterized where greater than 50% of the chemical diversity can be accounted for by combinations of either the dichloro-substituted acid or the alpha-cyano-3phenoxybenzyl alcohol moieties. Cypermethin and cyfluthrin, account for more than half of the data points.

It is worth noting, a lack of substituent diversity may limit our ability to model the influence of changes in acid and alcohol moieties on pyrethroid hydrolysis. Pyrethroids such as tralomethrin or even cyhalothrin with much larger acid moiety R-groups may not be well represented in our pharmacophore model. Diversity in R-group fragments of the alcohol moiety may also be lacking especially for cyclopentenolone and imidomethyl ester based pyrethroids (allethrin and phthalthrin) since 19 of the represented

structures are esters of alpha-cyano-3-phenoxybenzyl alcohol. While the dataset is far from complete, it is clear that the small number of data points specifically on seven pyrethroids (cypermethrin, cyfluthrin, permethrin, cyano-phenothrin, phenothrin, cyhalothrin and deltamethrin) will at a minimum describe aspects of rsCE mediated hydrolysis with respect to α -cyano and *cis/trans* isomers.

Structural bioinformatics

We posit two distinct mechanisms for ester cleavage of pyrethroids: i) a facile, rsCE catalytically enabled process (*i.e.*, rapid metabolism) and ii) a slower, non-specific process or what might be termed a “non-rsCE mediated metabolism route” or sterically hindered, catalytically “incompetent” mechanism. These two mechanisms conform to our use of two different pharmacophore models to characterized ligands for each process. To maximize our dataset and avoid potential ambiguities in metabolic specificity, we define stereoisomers as those most likely to undergo rapid metabolism exhibiting hydrolysis rates greater than 1.0 hr^{-1} , or $t_{1/2} < 34 \text{ min}$. This selection process results in 12 actives and 15 inactive structures. For slow metabolism, the inverse definition was adopted resulting in 15 actives and 12 inactive structures. Overall performance was 93% (100% actives : 87% inactives) and 96% (93% actives : 100% inactives) correct classification for rapid and slow metabolism models, respectively. The classification accuracy of the rapid metabolism model was increased to 100% with the addition of an exterior van der Waals volume determined from the structural alignment of the 12 actives. With the slow metabolism model, only 14 of the 15 active structures were correctly classified. The final model features are depicted in Figure 4.

Since neither crystal structure nor protein sequence was available for rsCE, docking calculations were performed on a homology modeled rat liver carboxylesterase developed from the

alignment and minimization of the CES3 protein sequence(47). Identification of what we determined as “competent” and “incompetent” poses were made based on their proximal distance to the SER-HIS-GLU catalytic triad and the purported GLY-GLY residue interaction near the carbonyl oxygen atom. With the analysis of docking energetics and relative population of poses, we observed a characteristic protein ligand interaction fingerprint indicative of the 2 types. Competent poses were characterized by proximal H-bond interactions with the carbonyl moiety and presented itself relatively close to the catalytic triad. In contrast, non-catalytically enabled poses were characterized by the lack of hydrogen bond interactions on carbonyl moiety as well as a lack of proximity of the carbonyl relative to the catalytic triad. In fact, many of the key interaction fingerprints of incompetent poses were characterized by interactions with the α -cyano group in Type II pyrethroids. Figure 5 illustrates a representative PLIF(48) pattern for incompetent and competent dock poses.

Chemoinformatics: QSAR model

Solvent (*i.e.*, water) accessible surface area on the [O]xygen atoms of the carbonyl moiety was calculated directly within MOE through an in-house developed SVL script. This conformation dependent parameter was estimated as the accessible surface area available to a spherical probe with a radius of 1.4 Å (*i.e.*, spherical “water”). More than 200 standard 2D and 3D molecular descriptors from the MOE’s QuaSAR module were calculated. Three of these 3D conformation-dependent molecular descriptors: [1] total solvent accessible surface area (*SASA*) in Å², [2] semiempirical AM1 dipole moment (μ) in units of Debye, and [3] van der Waals area (A_{vdw}) in Å²], were selected for inclusion in the two models. Two additional 2D conformation-independent molecular descriptors: [1] log of the aqueous solubility (log *S*) and [2] log of the octanol-water partition (log *P*) were also selected.

Both standard covariance matrix and variance inflation factor (VIF)(49) were used to determine whether individual molecular descriptors were highly correlated (>0.8) with other independent variables in our developed QSAR models. Anything with a VIF greater than five corresponding to a correlation of 0.8 was considered highly correlated and rejected from our analysis. QSAR models were generated to predict both rapid and slow metabolism based on the filtered data. We used the final 12 and 14 pharmacophore model selected 3D conformers as training sets for rapid and slow metabolism, respectively. The final bimodal consensus QSAR model was obtained:

$$(1) \log t_{1/2} = a_{rapid} * \log t_{1/2,rapid} + a_{slow} * \log t_{1/2,slow}$$

$$[n = 26, r^2 = 0.957, RMSE = 0.145]$$

where a_{rapid} and a_{slow} define a pharmacophore activity coefficient (*i.e.*, “1” is active and “0” is inactive) and $\log t_{1/2,rapid}$ and $\log t_{1/2,slow}$ are defined by:

$$(2) \log t_{1/2,rapid} = - 4.687482 - 0.120871 * SASA_{O=} - 0.43023 * \log P + 0.02861 * A_{vdw}$$

$$[n = 12, r^2 = 0.844, q^2 = 0.719, RMSE = 0.101, F = 24.4, p < 0.00025]$$

whereby the model for rapid metabolism is significantly more correlated than the one developed for slow metabolism:

$$(3) \log t_{1/2,slow} = 11.37051 - 0.0113 * SASA + 0.11743 * \mu - 0.01083 * SASA_{O=} + 0.24292 * \log S$$

$$[n = 14, r^2 = 0.577, q^2 = 0.195, RMSE = 0.174, F = 4.54, p < 0.03]$$

In Eqs 1 – 3, standard F statistics are reported in brackets when applicable and LOO cross validated q^2 as well as r^2 values and $RMSE$ values. The estimated relative importance of each descriptor was ascertained from individual slopes (beta coefficient $\beta^*(50)$) for each linear normalized regression (Figure 6). The regression for rapid metabolism emphasizes solvent accessible surface area on the carbonyl oxygen ($SASA_{O=}$) and van der Waals area (A_{vdw}). In contrast, the slow metabolism model emphasizes the total solvent accessible surface area ($SASA$) as well as the molecular dipole (μ) over $SASA_{O=}$. Interestingly, the form of both models suggests that $SASA_{O=}$ accounts for more of the variance in the rapid data vs. the slow data which is consistent with our interpretation of the pharmacophore model. In general, both regressions correlate negatively with $SASA_{O=}$ – *i.e.*, larger solvent accessible surface area about the carbonyl oxygen atom decreases the relative half live and increases the relative rate of hydrolysis.

The use of μ , $SASA$ and $\log S$ in the slow metabolism model could also be suggestive of a solvent-mediated hydrolysis process. However, the fact that the slow metabolic process showed relatively poor correlation (0.76) makes this argument less compelling. From the perspective of a high correlation rapid metabolism model (0.92), $\log P$ as an indicator of hydrophobicity and $SASA_{O=}$ are consistent descriptors within the context of the rapid pharmacophore model. Regardless, with high correlation (0.98), the overall consensus QSAR model given by Eq. 1 and depicted in Figure 7 suggests that rsCE metabolism of pyrethroids may best be described by a dual mechanism process (rapid vs. slow) largely influenced by stereochemistry. Our initial attempts to model the complete *in vitro* dataset proved challenging given that we were only able to account for at most 30% of the variance in the measured half-lives with a set of standard 2D descriptors.

It has been proposed(22-23, 51) that enzymatic CE hydrolysis occurs through a SER residue nucleophilic attack of the carbonyl carbon and that the intermediate is subsequently stabilized by

GLY-GLY residue interactions with the carbonyl oxygen (*i.e.*, H-bond stabilization of the oxyanion hole). This mechanism is consistent with both developed QSAR and pharmacophore models. Similar structure of the models suggests that both processes are mediated by a stabilization of the oxyanion hole (*i.e.*, $SASA_{O=}$ descriptor and *acc2* features in the QSAR and pharmacophore models, respectively). Similar location of the acceptor features (*acc2*) in both rapid and slow metabolism pharmacophore models could also suggest that the relative orientation of other features (*i.e.*, hydrophobic and aromatic) within the binding pocket modulate the relative rates of metabolism, which seems more restrictive for the slow metabolism mechanism than the rapid process. Both rapid and slow metabolism QSAR models are also suggestive of the importance in describing the carbonyl oxygen atom which is consistent with the emphasis on the $SASA_{O=}$ parameter in both models. The importance of parameters related to the carbonyl fragment for hydrolysis of esters has been recognized by Chaudry and Popelier(52) in their quantum topological molecular similarity method(53). Their study demonstrates that developed models for predicted base-promoted ester hydrolysis rates are highly influenced by the electron density about the C=O bond. Buchwald and Bodor adopted the notion of an inaccessible solid angle parameter, $\Omega_h^{O=}$, within their QSAR model which infers stereochemical as well as conformational information as a measure of steric hindrance around the carbonyl oxygen. However, this parameter, while significant in their model, is not necessarily specific to a true stereoselective description of the metabolic process. A ligand-based pharmacophore approach to actively discriminate amongst the available stereoisomers present in our training dataset potentially provides more rigor and substance to the idea of steric hindrance as a function of the conformational and specific stereoisomeric configuration of an enzyme substrate.

The developed dual mechanism-based model is promising given the limited dataset (*i.e.*, scope of chemical diversity). When coupled with the developed pharmacophore filter, we are able to

model the *in vitro* data as a bimodal “distribution” of carboxylesterase activity. However, it is clear that more work needs to be done to better understand the mechanics of this process. Further studies should be proposed such that 1) well-characterized stereoisomeric metabolism data is made available and 2) more rigorous *in silico* methods (*i.e.*, reaction following methods like QM/MM) should be employed to study the specific reaction mechanism in more detail.

CONCLUSIONS

Rapid *in silico* evaluation of pharmacokinetic parameters with respect to chemical specific ADME properties can provide a pivotal first step in developing a pharmacokinetic model especially in the case of little or no data. In the case of metabolism, stereoisomers of potential enzyme substrates are well known to exhibit stereoselective behavior in the homochiral protein environment. As such, the use of standard 2D molecular descriptors may not be sufficient enough to discriminate metabolic behavior between multiple stereoisomeric configurations. The process/workflow we've developed and adopted within this case study seeks to utilize a ligand-based pharmacophore approach to create a 3D conformer filter that takes into account explicit stereoisomeric configurations of potential substrates. The pharmacophore query behaves as a 3D chemical structure binary classifier for “non substrates” and “substrates” based on a user-defined cutoff and thereby allows one to quantify the metabolic behavior through the additional development of mechanistic-based QSAR with appropriate 2D and/or 3D molecular descriptors. Furthermore, the development of ligand-based pharmacophore filters enables one to posit the potential mechanism or salient molecular properties/features which might be necessary for describing characteristic metabolic behavior without explicit knowledge or information of the protein environment – a necessary challenge and endeavor since most enzyme kinetic mechanisms

and targets are neither well-studied nor well-characterized for a large number of chemicals and/or chemical classes.

For pyrethroid hydrolysis, we have illustrated a case example whereby two pharmacophore filters were developed to address the disparate metabolic behaviours (*i.e.*, rapid vs. slow metabolism) observed within *in vitro* data on rat serum carboxylesterase (rsCE) mediated hydrolysis. Homology modeled rsCE docking studies were performed to confirm differences in the observed behaviours. Protein ligand interaction fields (PLIF) were generated for prototypical poses found and we observed key features that corroborated the structural features of the pharmacophore query. One of the key findings in this study suggest that hydrogen bonding interactions with the backbone, specifically GLY-GLY residues, is a key indicator for rapid metabolism of specific stereoisomeric configurations of several pyrethroids in our dataset. This type of interaction is consistent with the *acc2* type features and *SASA_{O=}* descriptors given in both the pharmacophore and QSAR models. Furthermore, by applying the two pharmacophore filters, we were able to develop an informative consensus QSAR model with high selectivity for each mechanism and high overall correlation (0.98) with the observed kinetics given the limitations of the small dataset.

Ultimately, our goal in this case study is to illustrate the need of utilizing existing methods within computational chemistry to elucidate stereochemical effects especially with regards to metabolism. With the possibility of differential mechanics and targets, elucidating the complex behaviours of stereoselective metabolism becomes important in understanding the exposure-dose paradigm as it pertains to enantiopure and enantiomerically enriched (*i.e.*, mixtures) products and represents an important first step in the reduction of “isomeric ballast” (34) and more accurate PBPK/PD models. Forward momentum of models that handle metabolism of these chemicals is partially stifled by lack of appreciation for a means to resolve these problems. Neglect of

these chiral variables leads to the basis for Arien's "pharmacokinetic nonsense". Better characterization of the stereochemical implications on metabolism will lead to more informed models with regards to PBPK/PD model parameter development while reducing the uncertainty in human health risk assessment.

DISCLAIMER

This document has been subjected to review and approved for publication by the US EPA. Any use of trade, product, or firm names in this publication is for descriptive purposes only and does not imply endorsement by the US Government.

REFERENCES

1. Dennison, J. E.; Bigelow, P. L.; Mumtaz, M. M.; Andersen, M. E.; Dobrev, I. D.; Yang, R. S., *J Occup Environ Hyg* **2005**, *2* (3), 127-35.
2. Jang, J. Y.; Droz, P. O.; Kim, S., *Int Arch Occup Environ Health* **2001**, *74* (1), 31-7.
3. Clewell, H. J.; Gentry, P. R.; Gearhart, J. M.; Allen, B. C.; Andersen, M. E., *Sci Total Environ* **2001**, *274* (1-3), 37-66.
4. Cantoreggi, S.; Keller, D. A., *Toxicol Appl Pharmacol* **1997**, *143* (1), 130-9.
5. Corley, R. A.; Mendrala, A. L.; Smith, F. A.; Staats, D. A.; Gargas, M. L.; Conolly, R. B.; Andersen, M. E.; Reitz, R. H., *Toxicol Appl Pharmacol* **1990**, *103* (3), 512-27.
6. Loizou, G. D., *Toxicol Lett* **2001**, *124* (1-3), 59-69.
7. Tornero-Velez, R.; Rappaport, S. M., *Toxicol Sci* **2001**, *64* (2), 151-61.
8. Tan, Y. M.; Sobus, J.; Chang, D.; Tornero-Velez, R.; Goldsmith, M.; Pleil, J.; Dary, C., *J Toxicol Environ Health B Crit Rev* **2012**, *15* (1), 22-38.
9. Reddy, M.; Yang, R. S.; Andersen, M. E.; Harvey J. Clewell, I., *Physiologically Based Pharmacokinetic Modeling: Science and Applications*. John Wiley & Sons: 2005.
10. Nong, A.; Tan, Y. M.; Krolski, M. E.; Wang, J.; Lunchick, C.; Conolly, R. B.; Clewell, H. J., 3rd, *J Toxicol Environ Health A* **2008**, *71* (20), 1363-81.

11. Gelman, A.; Bois, F.; Jiang, J., *Journal of the American Statistical Association* **1996**, *91* (436), 1400-1412.
12. Eric Hack, C.; Chiu, W. A.; Jay Zhao, Q.; Clewell, H. J., *Regulatory Toxicology and Pharmacology* **2006**, *46* (1), 63-83.
13. Toxvaerd, S., *Int J Mol Sci* **2009**, *10* (3), 1290-9.
14. Siegel, J. S., *Nature* **2001**, *409* (6822), 777-778.
15. Saghatelian, A.; Yokobayashi, Y.; Soltani, K.; Ghadiri, M. R., *Nature* **2001**, *409* (6822), 797-801.
16. Ulrich, E. M.; Morrison, C. N.; Goldsmith, M. R.; Foreman, W. T., *Reviews of Environmental Contamination and Toxicology* **2012**, *217*, 1-74.
17. Chang, D. T.; Goldsmith, M. R.; Tornero-Velez, R.; Rabinowitz, J.; Dary, C. C., *Abstracts of Papers of the American Chemical Society* **2007**, *234*.
18. Knaak, J. B.; Dary, C. C.; Zhang, X.; Gerlach, R. W.; Tornero-Velez, R.; Chang, D. T.; Goldsmith, M.-R.; Blancato, J. N., *Reviews of Environmental Contamination and Toxicology* **2012**, *219* (1), 376.
19. Kim, K.-B.; Anand, S. S.; Kim, H. J.; White, C. A.; Fisher, J. W.; Tornero-Velez, R.; Bruckner, J. V., *Toxicological Sciences* **2010**, *115* (2), 354-368.
20. Godin, S. J.; DeVito, M. J.; Hughes, M. F.; Ross, D. G.; Scollon, E. J.; Starr, J. M.; Setzer, R. W.; Conolly, R. B.; Tornero-Velez, R., *Toxicological Sciences* **2010**, *115* (2), 330-343.
21. Mirfazaelian, A.; Kim, K.-B.; Anand, S. S.; Kim, H. J.; Tornero-Velez, R.; Bruckner, J. V.; Fisher, J. W., *Toxicological Sciences* **2006**, *93* (2), 432-442.
22. Matsuo, T.; Mori, T., *Pyrethroids: From Chrysanthemum to Modern Industrial Insecticide*. Springer Verlag: 2012.
23. Huang, H.; Fleming, C. D.; Nishi, K.; Redinbo, M. R.; Hammock, B. D., *Chem Res Toxicol* **2005**, *18* (9), 1371-7.
24. Crow, J. A.; Borazjani, A.; Potter, P. M.; Ross, M. K., *Toxicol Appl Pharmacol* **2007**, *221* (1), 1-12.
25. Ross, M. K.; Borazjani, A.; Edwards, C. C.; Potter, P. M., *Biochem Pharmacol* **2006**, *71* (5), 657-69.
26. Kaneko, H., *Journal of Agricultural and Food Chemistry* **2010**, *59* (7), 2786-2791.
27. Miyamoto, J., *Environ Health Perspect* **1976**, *14*, 15-28.
28. Liu, W.; Gan, J.; Schlenk, D.; Jury, W. A., *Proceedings of the National Academy of Sciences of the United States of America* **2005**, *102* (3), 701-6.
29. Soderlund, D., *Archives of Toxicology* **2012**, *86* (2), 165-181.
30. Soderlund, D. M.; Clark, J. M.; Sheets, L. P.; Mullin, L. S.; Piccirillo, V. J.; Sargent, D.; Stevens, J. T.; Weiner, M. L., *Toxicology* **2002**, *171* (1), 3-59.
31. Scollon, E. J.; Starr, J. M.; Godin, S. J.; DeVito, M. J.; Hughes, M. F., *Drug Metab Dispos* **2009**, *37* (1), 221-8.
32. Godin, S. J.; Scollon, E. J.; Hughes, M. F.; Potter, P. M.; DeVito, M. J.; Ross, M. K., *Drug Metab Dispos* **2006**, *34* (10), 1764-71.

33. Godin, S. J.; Crow, J. A.; Scollon, E. J.; Hughes, M. F.; DeVito, M. J.; Ross, M. K., *Drug Metabolism and Disposition* **2007**, *35* (9), 1664-1671.
34. Ariëns, E. J., *Quantitative Structure-Activity Relationships* **1992**, *11* (2), 190-194.
35. Mishra, N. K., *Expert Opinion on Drug Metabolism & Toxicology* **2011**, *7* (10), 1211-1231.
36. Ekins, S.; Swaan, P. W., Development of Computational Models for Enzymes, Transporters, Channels, and Receptors Relevant to ADME/Tox. In *Reviews in Computational Chemistry*, John Wiley & Sons, Inc.: 2004; pp 333-415.
37. Zou, J.; Xie, H.-Z.; Yang, S.-Y.; Chen, J.-J.; Ren, J.-X.; Wei, Y.-Q., *Journal of Molecular Graphics and Modelling* **2008**, *27* (4), 430-438.
38. Wermuth, C. G.; Ganellin, C. R.; Lindberg, P.; Mitscher, L. A., *Pure and Applied Chemistry* **1998**, *70* (5), 1129-1143.
39. Sippl, W., Pharmacophore Identification and Pseudo-Receptor Modeling. In *The Practice of Medicinal Chemistry*, 3rd ed.; Wermuth, C. G., Ed. Academic Press: 2008; pp 572-586.
40. Provost, F.; Kohavi, R., *Machine Learning* **1998**, *30* (2), 271-274.
41. Chen, L.-J.; Ulrich, E. M.; Lindstrom, A. B., unpublished data. 2012.
42. Chemical Computing Group, I. *Molecular Operating Environment (MOE)*, 2011.10; Chemical Computing Group, Inc.: 2011.
43. Halgren, T. A., *Journal of Computational Chemistry* **1996**, *17* (5-6), 490-519.
44. Labute, P., *Journal of Chemical Information and Modeling* **2010**, *50* (5), 792-800.
45. Kolossváry, I.; Guida, W. C., *Journal of the American Chemical Society* **1996**, *118* (21), 5011-5019.
46. Goto, J. *AutoQuaSAR 2006.8*, Ryoka Systems, Inc.: Tokyo, Japan, 2006.
47. <http://www.uniprot.org/>.
48. Clark, A. M.; Labute, P., *Journal of Chemical Information and Modeling* **2007**, *47* (5), 1933-1944.
49. O'Brien, R., *Quality & Quantity* **2007**, *41* (5), 673-690.
50. Pindyck, R. S., *Econometric Models and Economic Forecasts*. 1981.
51. Buchwald, P.; Bodor, N., *Journal of Medicinal Chemistry* **1999**, *42* (25), 5160-5168.
52. Chaudry, U. A.; Popelier, P. L. A., *The Journal of Physical Chemistry A* **2003**, *107* (22), 4578-4582.
53. O'Brien, S. E.; Popelier, P. L. A., *Journal of Chemical Information and Computer Sciences* **2001**, *41* (3), 764-775.

FIGURE CAPTIONS

Figure 1. *In silico* workflow. For modeling consistency, “activity” implies being a substrate (*e.g.*, rapid metabolism, whereas slow metabolism or “inactivity” imply different mode of kinetics, and thus a non-substrate. “1” represents the curation of a viable dataset into “active” and “inactive” subsets and the generation of possible conformers, “2” represents the development of a pharmacophore query on the basis of the selection criteria used to parse the subsets, and “3” represents the development of a QSAR model based on the selection criteria for both subsets. Post development, a test set can be used to predict and/or validate the model output.

Figure 2. Sprague-Dawley rat *in vitro* data for hydrolysis rates (k_h) and reaction half lives ($t_{1/2}$) in log units. The dashed line with Δ markers and the solid line with \bullet markers represent reported $\log k_h$ and $\log t_{1/2}$ values, respectively. The indices along the ordinate axis correspond to the structures in Figure 3.

Figure 3. 2D molecular representation of the chemical structures for the 27 pyrethroid stereoisomers used as a training set to generate pharmacophore and QSAR models. The top portion of each box is identified by an index number next to the stereochemistry with respect to the C1 of the cyclopropane ring [*IR*, *IS*], the relative stereochemistry about the C1-C3 bond of the cyclopropane ring [*cis*, *trans*], and the stereochemistry of the α -C if a cyano group is present [α -*S*, α -*R*] (*i.e.*, Type II pyrethroids). At the bottom of each box, the generic pyrethroid name is given for reference.

Figure 4. Schematic illustration of elucidated 5 point pharmacophore models for (a) rapid and (b) slow metabolism. Model (a) is shown with the “fastest” metabolized ligand (*IR*, *trans*, α -*R* cypermethrin) and model (b) is shown with the “slowest” metabolized ligand (*IS*, *cis*, α -*S* cypermethrin). Ligand-centered projections (*acc2*) are illustrated as vector arrows

originating from the respective atom centers. Green, orange and cyan spheres represent Hydrophobic (*Hyd*), Aromatic (*Aro*) or π ring center (*PiR*), and H-bond acceptor projection (*acc2*) respectively.

Figure 5. Docked poses and Protein-Ligand Interaction Fingerprints (PLIF) for [*1S*, *trans*, α -*R*] cypermethrin: (i) 2D generated PLIF for (a) “competent” and (b) “incompetent” poses, and (ii) 3D representations of (a) and (b) poses within the binding cavity showing proximity to SER-HIS-GLU catalytic triad (in red) and GLY-GLY residues (in blue). The 2D PLIF illustrates interactions with GLY residue mimicking H-bond acceptor type interaction in the pharmacophore query. 3D representation below illustrates the relative location of the pyrethroid (space filling representation) to SER and GLY-GLY residues. In (a), the SER and GLY proximity with the carbonyl group suggests key fingerprints for catalytically enabled poses. In (b), SER interaction with the α -cyano group suggests a competitive process that may not promote ester hydrolysis in rsCE. More information regarding PLIF representations can be found in Clark and Labute(48).

Figure 6. Relative importance of molecular descriptors in developed QSAR models. White and black bars represent rapid and slow metabolism QSAR models, respectively. Descriptor names are defined in the text and are displayed on the ordinate axis.

Figure 7. Predicted vs. observed *in vitro* rat serum carboxylesterase hydrolysis half lives in log units using the developed QSAR consensus model based on a bimodal mechanism of rapid and slow metabolism defined by Eqs. 1 – 3.

Figure 1.

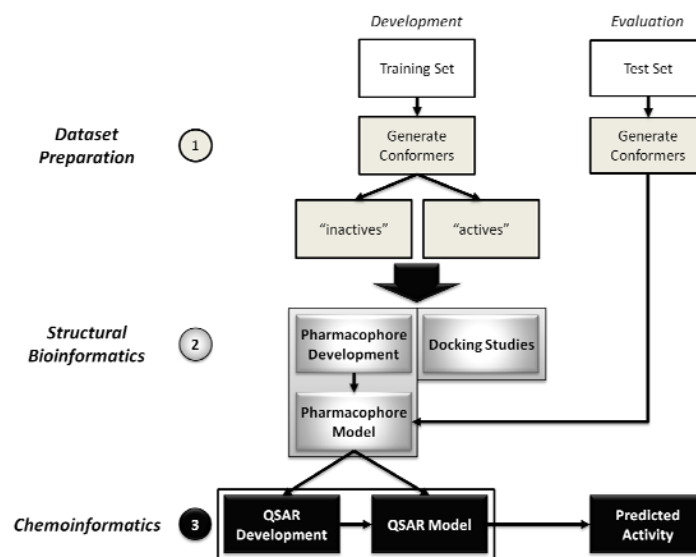


Figure 2.

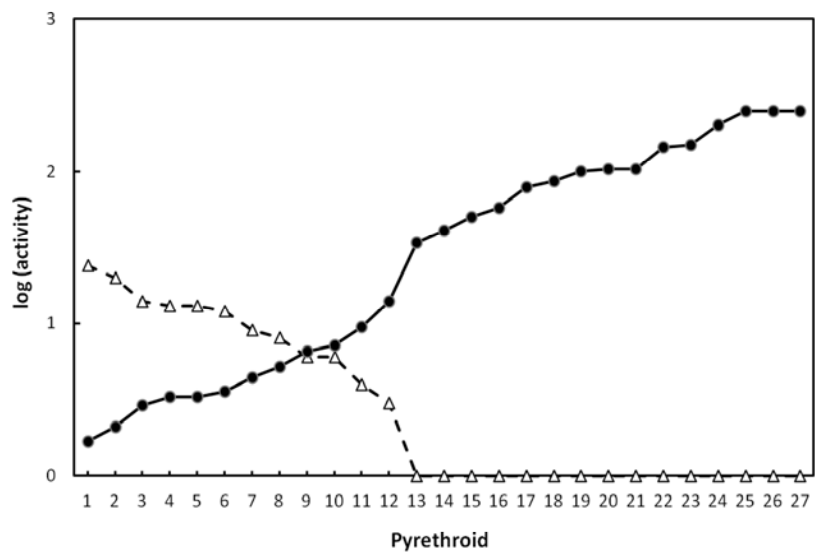


Figure 3.

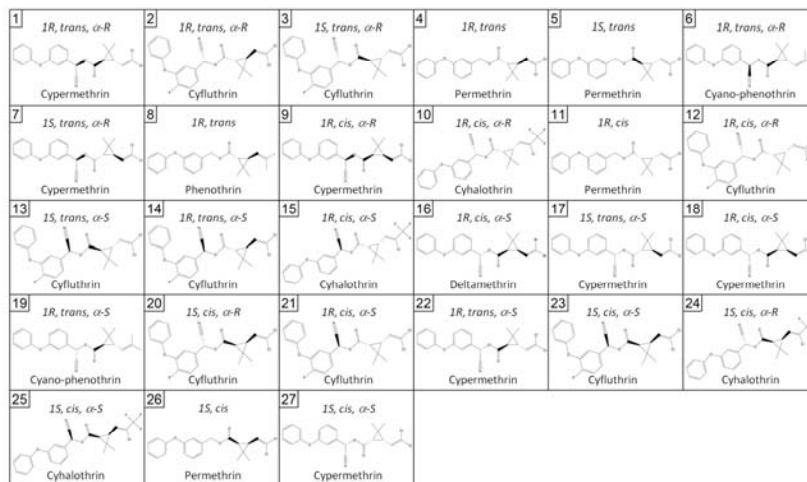


Figure 4.

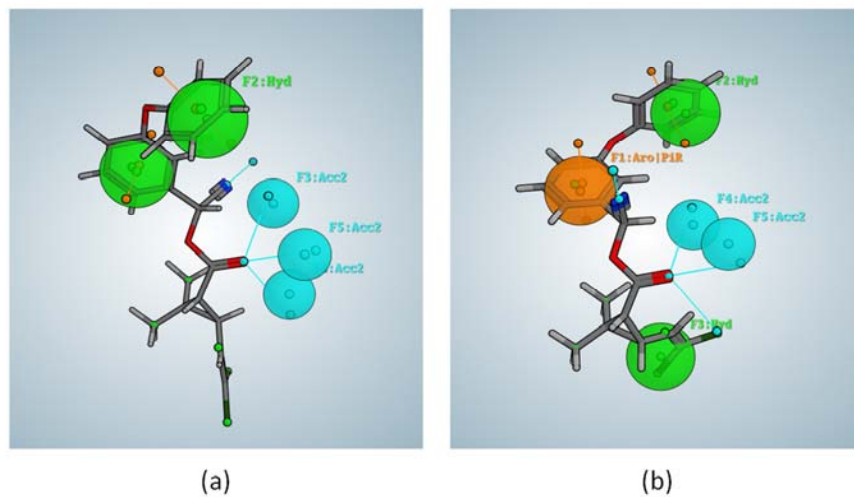


Figure 5.

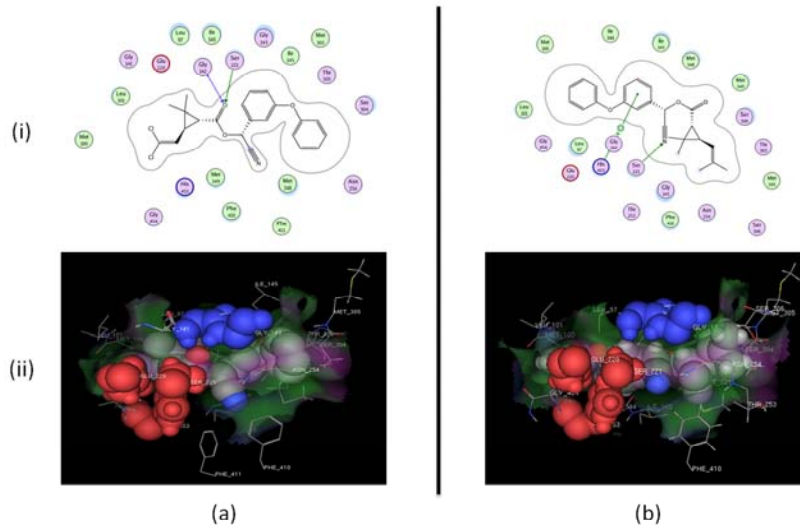


Figure 6.

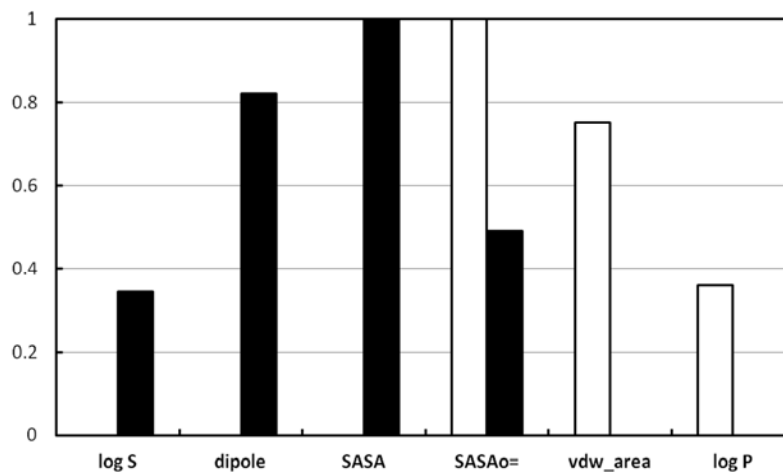


Figure 7.

